Experiments in Fluids 28 (2000) 266–278 © Springer-Verlag 2000

Turbulent characteristics of shear-thinning fluids in recirculating flows

A. S. Pereira, F. T. Pinho

Abstract A miniaturised fibre optic Laser-Doppler anemometer was used to carry out a detailed hydrodynamic investigation of the flow downstream of a sudden expansion with 0.1–0.2% by weight shear-thinning aqueous solutions of xanthan gum.

Upstream of the sudden expansion the pipe flow was fully-developed and the xanthan gum solutions exhibited drag reduction with corresponding lower radial and tangential normal Reynolds stresses, but higher axial Reynolds stress near the wall and a flatter axial mean velocity profile in comparison with Newtonian flow. The recirculation bubble length was reduced by more than 20% relative to the high Reynolds number Newtonian flow, and this was attributed to the occurrence further upstream of high turbulence for the non-Newtonian solutions, because of advection of turbulence and earlier high turbulence production in the shear layer.

Comparisons with the measurements of Escudier and Smith (1999) with similar fluids emphasized the dominating role of inlet turbulence. The present downstream turbulence field was less anisotropic, and had lower maximum axial Reynolds stresses (by 16%) but higher radial turbulence (20%) than theirs. They reported considerably longer recirculating bubble lengths than we do for similar non-Newtonian fluids and Reynolds numbers.

Received: *23 February 1999/ Accepted*: *28 April 1999*

A. S. Pereira,
Departamento de Engenharia Quimića,
Instituto Superior de Engenharia do Porto,
Rua de S. Tomé, 4200 Porto,
Portugal

F. T. Pinho
Centro de Estudos de Fenómenos de Transporte,
Departamento de Engenharia Mecânica e Gestão Industrial,
Faculdade de Engenharia da Universidade do Porto,
Rua dos Bragas, 4050-123 Porto,
Portugal

Correspondence to: F. T. Pinho

The authors acknowledge the financial support of JNICT-Junta Nacional de Investigação Científica-through contract number PBIC/C/CEG/2427/95, the donation by the Stichting Fund of Schlumberger and the facilities provided by INEGI-Instituto de Engenharia Mecânica e Gestão Industrial. The helpful discussions with Prof. M. P. Escudier and Miss S. Smith from the University of Liverpool, are also gratefully acknowledged. The author's names are listed alphabetically.

Nomenclature

C_T	static pressure variation coefficient
D	diameter of pipe downstream of sudden expansion [m]
d	diameter of pipe upstream of sudden expansion [m]
ER	expansion ratio
f_D	Darcy friction factor
h	step height [m]
K	consistency index in power law model [Pas^n]
k	turbulent kinetic energy [m^2/s^2]
L	recirculation bubble length [m]
n	power law index in power law and Sisko viscosity models
R	radius of pipe [m]
Re	Reynolds number (Eq. (2))
Re_w	Reynolds number based on wall viscosity in the upstream pipe
Re_{gen}	generalised Reynolds number (Eq. (4))
r	local radius [m]
U	axial bulk velocity [m/s]
U_{in}	axial bulk velocity at inlet [m/s]
u	local axial mean velocity [m/s]
U_0	axial centreline velocity [m/s]
U^+	local maximum velocity in the shear layer [m/s]
U^-	local minimum velocity in the shear layer [m/s]
u'	local root mean square of axial velocity [m/s]
v'	local root mean square of radial velocity [m/s]
w'	local root mean square of tangential velocity [m/s]
x	longitudinal coordinate [m]
β	shape factor for momentum
γ_e	stored shear deformation in creep test [m/m]
γ_t	total shear deformation in creep test [m/m]
$\dot{\gamma}$	shear rate [s^{-1}]
η_{ref}	reference viscosity in the Sisko model [Pas]
η_∞	infinite shear rate viscosity in the Sisko model [Pas]
λ	time constant of Sisko viscosity model [s]
ρ	fluid density [kg/m^3]
σ	area ratio
μ	fluid viscosity [Pas]
μ_w	viscosity at the wall in the upstream pipe [Pas]

Subscripts

1	refers to upstream pipe
2	refers to downstream pipe

ch	refers to a characteristic value
in	refers to characteristic values at the inlet pipe
max	refers to maximum values

1 Introduction

The vast majority of turbulent flow research with non-Newtonian fluids has concentrated on understanding wall-dominated flows with polymer solutions and more recently surfactants (Gyr and Bewersdorff (1995) covers both extensively), but a better knowledge and understanding of turbulent flow behaviour requires also the investigation of wall-free flows, preferably with the same fluids as used in wall experiments. The axisymmetric sudden expansion flow is easily implemented for liquid flows and has been extensively investigated in the past for Newtonian fluids, especially in the last quarter of the century, due to its relevance in a number of practical situations, such as burner and diffuser development.

The main features of a sudden expansion flow are qualitatively independent of the fluid rheology, therefore knowledge of the Newtonian case is helpful in the analysis. Sudden expansion flows and flows through orifices were first investigated by Chevalier de Borda in 1766 (Rouse and Ince 1957; Tokaty 1971). In particular, Borda investigated the discrepancies observed in sudden expansion flows concerning the area-velocity-pressure relationships of the Bernoulli–Lagrange law[1] and da Vinci's continuity relationship[2] which lead to the statement of the Borda theorem and the introduction of the concept of flow separation. A concise summary of recent research for Newtonian fluid through sudden expansions at high Reynolds numbers and various inlet conditions is presented by Devenport and Sutton (1993), with the low Reynolds number cases covered by Oliveira and Pinho (1997) and Drikakis (1997), amongst others. The literature surveys of the last two papers emphasize recent research results relying on modern non-intrusive experimental techniques.

Wall-free turbulent flow investigations with non-Newtonian fluids, and in particular the sudden expansion case, are rather scarce. Pak et al. (1990,1991) showed the influences of fluid viscosity and elasticity on the mean flow characteristics of Carbopol and Separan solutions under laminar, transitional and turbulent conditions, but failed to report detailed turbulent measurements in the latter case. In 1995 Castro and Pinho mapped the mean and turbulent fields of the sudden expansion flow of weakly elastic 0.4% and 0.5% by weight aqueous solutions of tylose (molecular weight of 6000 kg/kmol), which were previously investigated by Pereira and Pinho (1994) regarding their fully-developed turbulent pipe flow characteristics. These solutions were found to be inelastic in conventional rheometric shear tests, but showed drag reductions up to 24% and 27% in turbulent pipe flow, respectively. The polymer solutions resulted in small variations in the recirculation bubble length and reductions of the normal Reynolds stresses of up to 30%, especially in the tangential and radial directions relative to the corresponding Newtonian flows. The reader is referred to Castro and Pinho (1995) for a summary of the remaining literature on non-Newtonian expansion flows, excluding creeping flows. Research on other wall-free turbulent flows of non-Newtonian fluids, such as jets, shear layers or decay of grid generated turbulence are even scarcer and the review by Pinho (1990) is still up to date.

The extension of the sudden expansion flow research to other fluids and different inlet conditions is thus deemed necessary to enhance our understanding of the physical phenomena. In particular, the research should be extended to various types of fluids, such as shear-thinning fluids exhibiting elasticity effects in shear flows and higher levels of drag reduction in turbulent pipe flow and to different inlet flow conditions. Examples of such fluids are, for instance, the aqueous solutions of xanthan gum tested by Escudier et al (1995) or the CMC solutions of Pinho and Whitelaw (1990). The investigation of sudden expansion flows of xanthan gum based fluids constitutes the objective of a common research programme, the results of which are being reported here and by Escudier and Smith (1999): in this joint research similar Newtonian and non-Newtonian fluids and identical sudden expansions will be used, but whereas here the inlet flow condition is fully-developed, a uniform velocity inlet with a low turbulence intensity profile was used by Escudier and Smith (1999).

In the next section the rig and instrumentation are described. The characteristics of the fluids are presented in Sect. 3 and followed by the presentation and discussion of results with emphasis on Reynolds number and non-Newtonian effects. The experimental data are compared throughout this paper with those of Escudier and Smith (1999) in order to assess the influence of the inlet flow condition. The paper ends with a summary of the main conclusions.

2 Experimental set up

The flow configuration is similar to that used in the sudden expansion experiments of Castro and Pinho (1995) and is depicted in Fig. 1. The installation consisted of a vertical closed loop with a 100 litre tank and a centrifugal pump located at the bottom. The descending pipe before the test section was 26 mm in diameter and more than 90 diameters long, leading to a transparent sudden expansion test section from 26 to 40 mm in diameter and 700 mm in length. The 40 mm diameter pipe downstream of the test section was fitted with a valve and led the flow back to the tank. The test section had a square outer cross section to reduce diffraction of light beams. A honeycomb was placed at the beginning of the descending 26 mm pipe, located 90 diameters upstream of the sudden expansion plane, to help ensure a fully developed flow at the inlet of the sudden expansion.

The rising pipe had an electromagnetic flowmeter (model Mag Master from ABB Kent-Taylor) and its output signal was recorded on a computer via one of the channels of a data acquisition board Metrabyte DAS-8 interfaced with a

[1] According to Tokaty (1971) Bernoulli was the first to recognize that an increase in velocity leads to a definite decrease in pressure, but not in the way predicted by the formula ascribed to him in every textbook. That formula, called here the Bernoulli–Lagrange law, was Lagrange's integral of Euler's equation of motion.

[2] According to Tokaty (1971) Leonardo was one of the first to exploit the interdependence of the cross-sectional area of a flow and its velocity.

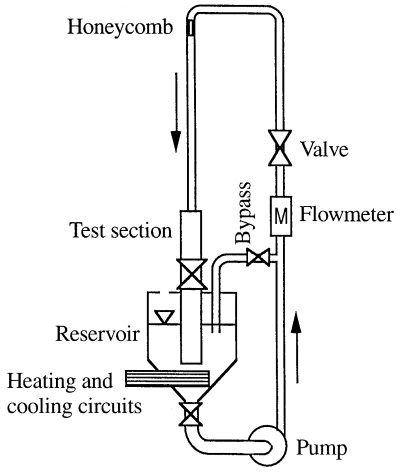

Fig. 1. Schematic representation of the experimental rig

Metrabyte ISO 4 multiplexer, both from Keithley. The two valves on the main loop and a third on the bypass allowed the flow rate to be controlled. The measured flow rates were found to be within 2% of values computed from the velocity profiles when these were measured from wall to wall. The connection between the brass pipe and the test section was carefully manufactured with machining tolerances of ± 10 μm.

Fourteen pressure taps were located on the pipe downstream of the sudden expansion and two taps were drilled upstream, in the region of fully-developed flow. The pressure variation in the sudden expansion was measured by means of differential pressure transducers from Validyne (models P305D S20 and S24) and their outputs were sent to a computer via the same data acquisition board as used for the flow rate measurements. The overall uncertainty of the pressure measurements varied between 1.6% and 7.2% for high and low pressure differences, respectively.

Heating and cooling circuits in the reservoir were used to control and maintain the temperature at a constant 25°C.

For the velocity measurements a miniaturised fiber optics laser-Doppler velocimeter from INVENT, model DFLDA similar to that described by Stieglmeier and Tropea (1992), was used with a 100 mm front lens mounted onto the 30 mm diameter probe. Scattered light was collected by a photodiode in the forward scatter mode, and the main characteristics of the anemometer are listed in Table 1. Measurements of the radial velocity component were limited to the inner 70% of the pipe radius due to excessive refraction of light beams outside that region.

The signal was processed by a TSI 1990C counter interfaced with a PC via a DOSTEK 1400 A card, which provided the statistical quantities based on 4000 realisations. The data presented in this paper have not been corrected for the effects of the mean gradient broadening and the maximum uncertainties in the axial mean and rms velocities at a 95% confidence level are 1.0% and 2.2% on axis and 1.1% and 5.2% in the wall region, respectively. The uncertainty of the radial and tangential rms velocity components is 2.5% on axis and 5.9% close to the wall.

The velocimeter was mounted on a milling table with movement in the three coordinates and the positional uncertainties are ± 200 and ± 150 μm in the axial and transverse directions, respectively.

Table 1. Laser-Doppler characteristics

Laser wavelength	827 nm
Laser power	100 mW
Measured half angle of beams in air	3.68°
Measuring volume size in water (e^{-2} intensity)	
minor axis	37 μm
major axis	550 μm
Fringe spacing	6.44 μm
Frequency shift	2.5 MHz

3 Fluid properties

Water and aqueous solutions of xanthan gum grade Keltrol TF from Kelco, a polysaccharide of high molecular weight (2×10^6 kg/kmol), at weight concentrations of 0.1% and 0.2% were used. This additive produced solutions of higher elasticity than those of the CMC of Pinho and Whitelaw (1990) and the tylose of Castro and Pinho (1995), but at the same time the solutions were more shear-thinning especially at low shear rates. The polymer was dissolved in tap water and 0.02% by weight of the biocide Kathon LXE from Rohm and Haas was added to help prevent bacteriological degradation. The rheological characterisation was carried out in the Physica MC 100 rheometer implementing a double gap concentric cylinder geometry. A new batch of fluid was made whenever the degradation led to a decrease in the viscometric viscosity exceeding 10% which corresponded to about 50 hours of pumping in the rig.

The viscometric viscosity of the solutions are plotted in Fig. 2 together with the curve-fitted Sisko model equation (Eq. (1)) whose parameters are listed in Table 2. The crosses represent the viscosity of Escudier and Smith's (1999) 0.2% xanthan gum solution. The differences are of the order of 30% at shear rates of 2 s^{-1}, decreasing to about 15% at 1000 s^{-1}. The larger difference at low shear rates is irrelevant under conditions of turbulent flow. The above result was unexpected since the previous rheological measurements of 0.25% aqueous solutions of xanthan gum, carried out simultaneously in our Physica MC100 rheometer and the Bohlin VOR concentric cylinder at the University of Liverpool, showed negligible differences in viscosity (Escudier et al, 1998). The viscometric viscosity and the loss and storage moduli were measured in that work and it was found that, for the range of shear rates of relevance to this work ($\dot{\gamma} > 0.1$ s^{-1}), there was a negligible influence of the solvent (tap water from Porto or Liverpool) upon the rheology of the 0.25% xanthan gum solution.

$$\eta = \eta_{\mathrm{ref}} (\lambda_s \dot{\gamma})^{n-1} + \eta_\infty \tag{1}$$

Creep and oscillatory tests were carried out to assess the elasticity of the solutions. In the creep tests the ratio of the stored shear deformation γ_e to the total deformation γ_t of the 0.1% and 0.2% xanthan gum solutions was less than 0.04% and 0.15%, respectively for a range of applied shear stresses between 0.3 and 3 Pa. In the oscillatory shear tests it was not possible to get reliable data for amplitudes of deformation

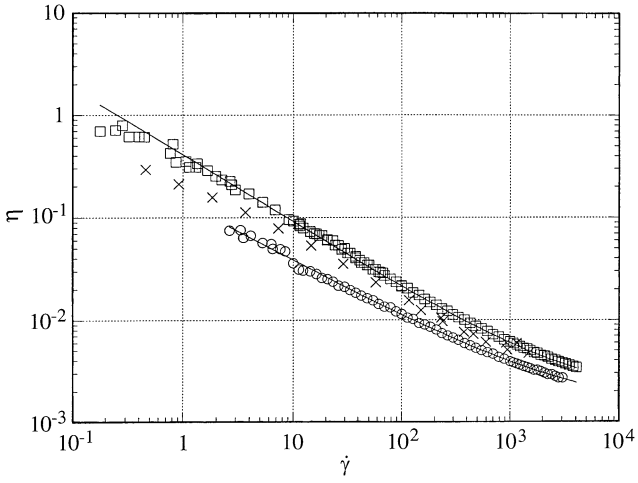

Fig. 2. Viscometric viscosity of the xanthan gum solutions and the corresponding curve fitted Sisko models. ○ 0.1% xanthan gum, □ 0.2% xanthan gum; × 0.2% xanthan gum measured by Escudier and Smith (1999)

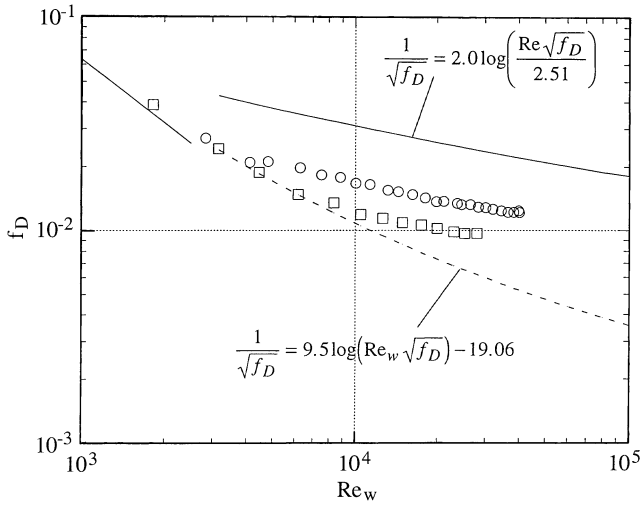

Fig. 3. Darcy friction factor as a function of the wall Reynolds number in a fully developed pipe flow. ○ 0.1% xanthan gum, □ 0.2% xanthan gum

Table 2. Sisko model parameters for Keltrol solutions at 25 °C

Solution	η_{ref} [Pas]	η_∞ [Pas]	λ_s [s]	n
0.1%	10.5	0.0012	1970	0.43
0.2%	58.1	0.0016	1900	0.34

below 0.2, for which the ratio of the storage to loss moduli G'/G'' was less than 0.7 for the 0.1% solution and about 1 for the 0.2% solution. These results show a comparatively more elastic behaviour than the tylose and CMC solutions of Pereira and Pinho (1994) and Pinho and Whitelaw (1990), respectively and it can thus be expected a higher degree of drag reduction in turbulent pipe flow for the xanthan gum solutions. There is at present no theory linking quantitatively γ_e/γ_t or G'/G'' to such non-Newtonian flow phenomena as drag reduction which is usually associated to elongational effects (Gyr and Bewersdorff 1995) and often, but not always, fluids exhibiting higher elasticity in shear flow will be more elastic in elongational flows. So, in the absence of elongational viscosity measurements we have to rely on other measurements of elastic quantities. The widest possible rheological characterisation is also essential for fitting complex constitutive equations to the experimental data for the purpose of future investigations on turbulence modelling of complex flows with non-Newtonian fluids.

The amount of drag reduction of the two xanthan gum solutions in turbulent pipe flow is shown in Fig. 3 for a 26 mm diameter pipe. Maximum wall Reynolds numbers of 40,100 and 28,100 were reached, for which drag reductions of 45% and 59% were measured for the 0.1% and 0.2% xanthan gum solutions, respectively. These values represent over 50% and 75% of the maximum drag reduction predicted by Virk's asymptote (Virk et al. 1970) at the same Reynolds numbers. They are also substantially higher than those reported by Pereira and Pinho (1994) for identical weight concentrations of tylose, but are similar to those of Pinho and Whitelaw (1990) with solutions of CMC. As a drag reducer these xanthan gum solutions are less efficient than very dilute solutions based on highly flexible polymer molecules of similar molecular weight, such as polyethylene oxide or polyacrylamide, but are significantly more resistant to mechanical degradation. The turbulent pipe flow behaviour of the xanthan gum solutions also suggests that its turbulent flow field downstream of the expansion will exhibit a stronger turbulence dampening and a higher degree of Reynolds stress anisotropy than observed by Castro and Pinho (1995) with tylose solutions, but only marginally so relative to the CMC solutions. Such comparison between the sudden expansion flow behaviour of xanthan gum and CMC solutions will be reported in the future.

4 Results and discussion

Five flow conditions were investigated in detail and allowed the analysis of the effects of Reynolds number and additive concentration and, by comparison with Escudier and Smith (1999), the effect of inlet condition. The issue of Reynolds number definition in complex flows of variable viscosity fluids has already been discussed in some detail by Castro and Pinho (1995). To facilitate comparisons with previous works three Reynolds numbers are calculated for each flow condition and presented in Table 3: the Reynolds number based on the upstream bulk velocity and wall viscosity Re_w, the Reynolds number Re used by Castro and Pinho (1995) defined by Eqs. (2) and (3) and the generalised Reynolds number Re_{gen} of Eq. (4). The Reynolds number Re is defined here as

$$Re = \frac{\rho U_{\mathrm{in}} d}{\bar{\mu}(\dot{\gamma}_{\mathrm{ch}})} \tag{2}$$

where the viscosity is calculated with the Sisko model (Eq. (1)) at a characteristic shear rate $\dot{\gamma}_{\mathrm{ch}}$ involving the step height, here defined as

$$\dot{\gamma}_{\mathrm{ch}} \equiv \frac{U_{\mathrm{in}}}{h} \tag{3}$$

Table 3. Main flow characteristics of the investigated flows of water and xanthan gum (XG)

Run	Fluid	U_{in} [m/s]	Re	Re_w	Re_{gen}	L/h	$\overline{u^2_{max}}/U_1^2$	$\overline{w^2_{max}}/U_1^2$	$\overline{v^2_{max}}/U_1^2$	k^2_{max}/U_1^2
1	water	4.61	135,000	135,000	135,000	8.43	0.0466	0.0326	0.0275	0.0533
2	water	1.73	50,300	50,300	50,300	8.71	0.0423	0.0279	0.0271	0.0478
3	0.1% XG	3.04	14,200	19,600	8,100	6.93	0.0400	0.0321	0.0247	0.0481
4	0.2% XG	5.10	19,000	27,200	10,700	6.78	0.0516	0.0326	0.0256	0.0540
5	0.2% XG	4.05	13,400	19,400	7,700	7.14	0.0447	0.0325	0.0242	0.0499

The generalised Reynolds number is given by Eq. (4)

$$Re_{gen} = \frac{\rho D_1^n U_1^{2-n}}{K} \tag{4}$$

and is equivalent to using Eq. (2) with the Ostwald de Waele viscosity power law at characteristic shear rate of $\dot{\gamma}_{ch} = U_{in}/d$.

For each fluid the largest Reynolds number in Table 3 corresponds to the maximum flow rate in the rig. The table lists also the recirculation length L normalised by the step height h and the maximum values of the three normal Reynolds stresses and turbulent kinetic energy normalised by the square of the inlet bulk velocity. To measure the recirculation length the axial velocity was measured twice in a fine grid around the estimated location of flow reattachment and the data interpolated to find the location of zero mean axial velocity. The nodes of this grid were equally spaced axially and radially by 3 and 0.2 mm, respectively and the overall uncertainty of the recirculation bubble length measurement, due to positional and mean velocity uncertainties, is better than 3%.

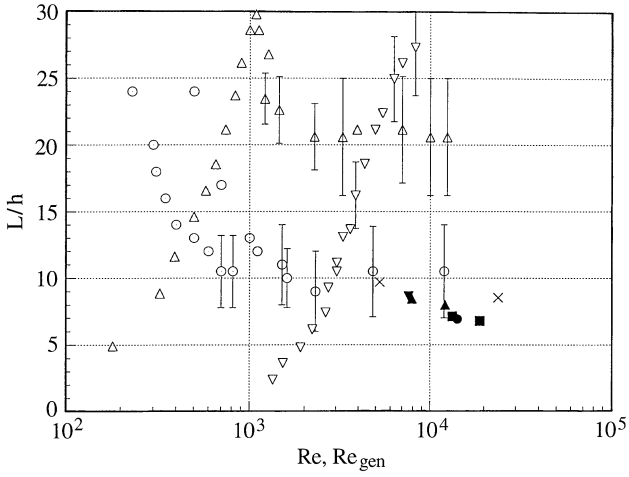

Fig. 4. Normalised recirculation length for non-Newtonian fluids. Pak et al. (1990) $D/d = 2.667$: ○ Carbopol 5000 ppm, ⊙ Carbopol 15,000 ppm; Pak et al. (1990) $D/d = 2.0$: △ Separan 200 ppm, ▽ Separan 1000 ppm; Castro and Pinho (1995) $D/d = 1.538$: ▲ 0.4% tylose, ▼ 0.5% tylose; Escudier and Smith (1999) × 0.2% xanthan gum; Present work $D/d = 1.538$: ● 0.1% xanthan gum, ■ 0.2% xanthan gum. The error bars are those of Pak et al. (1990); Separan and carbopol use Re_{gen}, other solutions use Re

4.1 Mean Flow

The normalised recirculation lengths for the Newtonian fluid compare well with the previous measurements of Castro and Pinho (1995) in this same rig of $L/h = 8.67$ for $Re = 178{,}000$, and also agree with other data in the literature taking into account the differences in expansion ratio and its corresponding effect (Khezzar et al. 1985).

Considering previous non-Newtonian results from the literature, the shorter recirculations with the xanthan gum solutions were quite unexpected. To the authors' knowledge there have been only three previous investigations of this quantity and their results, together with the present measured lengths, are plotted in Fig. 4. Initially we thought that non-Newtonian polymer solutions would exhibit similar or longer eddy sizes in comparison to the Newtonian values at identical Reynolds numbers in the turbulent regime, but this work shows that shorter bubbles can also occur. The values measured by Escudier and Smith (1999) for a plug velocity inlet with 0.2% xanthan gum are higher than ours and higher than the tylose measurements of Castro and Pinho (1995), also with a fully developed inlet. In the absence of turbulence, a flat inlet velocity profile enhances molecular diffusion in the shear layer relative to the fully developed flow case, hence the recirculation bubble will be shorter (Oliveira and Pinho 1997), but in turbulent flow the picture is rather different because of the dominating role of turbulence. Here, the plug velocity profile produced by the upstream contraction is associated with low turbulence levels. The radial momentum transfer downstream of the expansion will be dominated by the turbulent contribution which is locally produced, whereas in the fully-developed case local turbulence will benefit, in addition, from advection of turbulence from upstream. As a consequence, we expect larger fluxes of radial momentum at the beginning of the expansion for the latter case, ultimately leading to shorter recirculation lengths. Evidence for this will be presented later.

The differences between the present measurements and those of Castro and Pinho (1995) with tylose can also be explained on the basis of the location and magnitude of the maximum normal Reynolds stresses which are strongly dependent of the inlet condition. Therefore, it is extremely important to analyse first the inlet flow condition.

Pressure gradients measured between the two upstream pressure taps were in agreement with the pressure gradients measured with the same fluid in the straight pipe test section of Pereira and Pinho (1994). Fig. 5a shows the radial profiles of the mean axial velocity in the fully developed pipe flow at a station $0.5d$ upstream of the sudden expansion. The velocities were normalised by the centreline velocity and the profiles at higher Reynolds numbers are flatter than those at lower Reynolds numbers. The mean and turbulent Newtonian velocity profiles are in agreement with those in the literature (Laufer 1954; Lawn 1971), thus confirming a fully developed

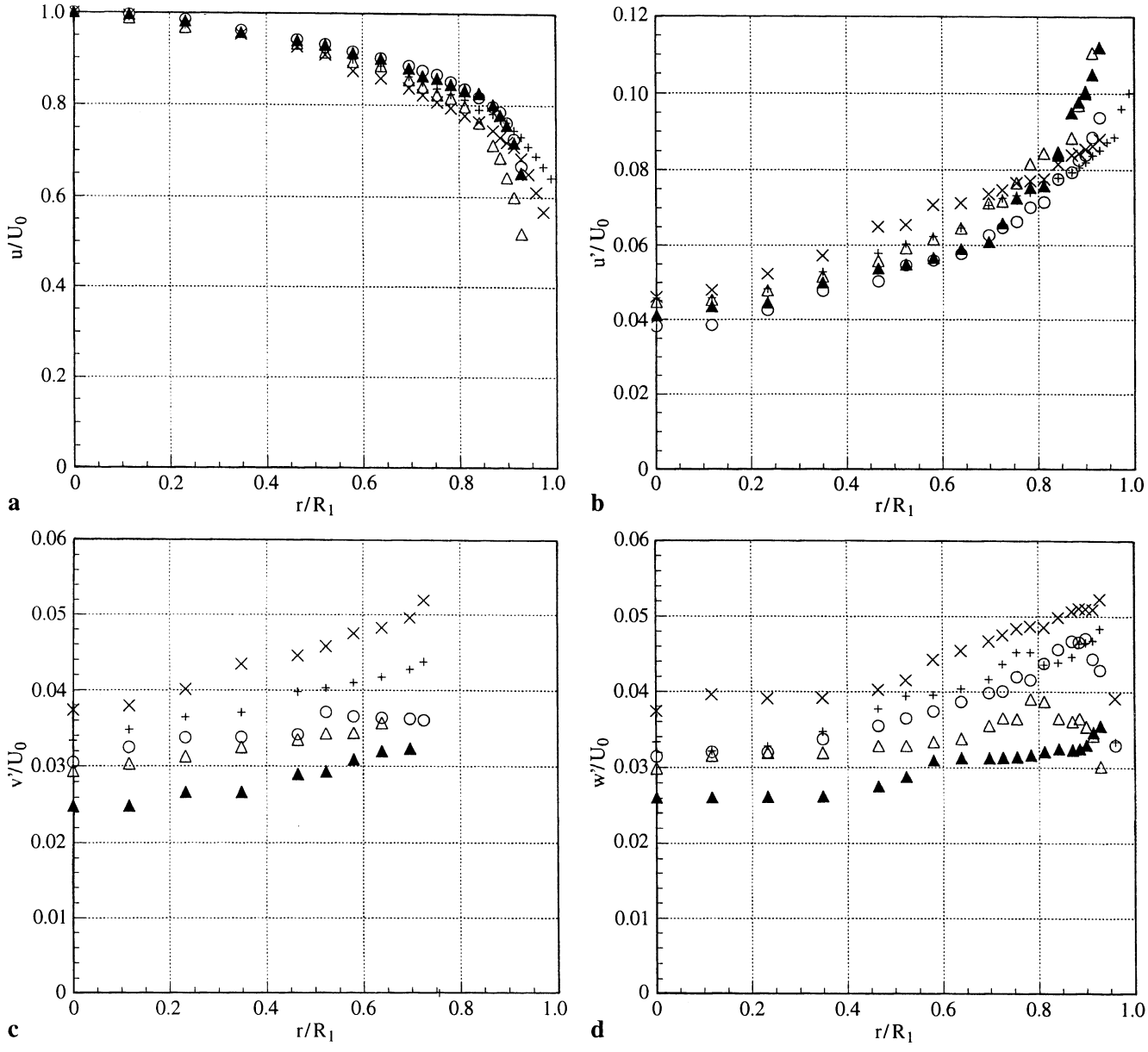

Fig. 5. Radial profiles of normalised mean velocity and rms of the fluctuating velocities at $x/d = 0.5$ upstream of the expansion. × water $Re = 50{,}300$; + water $Re = 135{,}000$; ○ 0.1% xanthan gum $Re_w = 19{,}600$; △ 0.2% xanthan gum $Re_w = 19{,}400$; ▲ 0.2% xanthan gum $Re_w = 27{,}200$. **a** Axial mean velocity; **b** Axial rms velocity; **c** Radial rms velocity; **d** Tangential rms velocity

flow condition at the inlet of the expansion and a negligible upstream influence of the sudden expansion.

The profiles for the 0.1% xanthan gum solution at $Re = 19{,}600$ and the 0.2% xanthan gum solution at $Re = 27{,}200$ are flatter than any of the Newtonian profiles, in spite of the significantly lower values of their Reynolds numbers.

The profiles of the rms of the velocities of the non-Newtonian fluids in Figs. 5b to d are typical of fluids exhibiting drag reduction. Both transverse components ($\overline{v'^2}$ and $\overline{w'^2}$) are considerably dampened in relation to that of their Newtonian counterparts. This effect is stronger than suggested by the figures when we account for the reduction of the low Reynolds numbers in fully-developed pipe flow which is normally associated with an increase in the turbulence (compare data for Newtonian flows at $Re = 50{,}300$ and $Re = 135{,}000$). However, the axial turbulence of the xanthan gum solutions is only slightly reduced in the core of the pipe but is considerably higher near the wall than that of the Newtonian flows. This difference between the behaviours of $\overline{u'^2}$ and of $\overline{v'^2}$ and $\overline{w'^2}$ is usually associated with a decoupling of the axial-transverse cross correlations which leads inevitably to a reduction of the friction factor in pipe flow.

The mean flow downstream of the expansion is depicted in Fig. 6 showing radial profiles of the normalised axial mean velocity. Fig 6a compares the flow field of the 0.1% xanthan gum solution with that of the water flows whereas Fig. 6b compares water and 0.2% xanthan gum. The lines in the figures show the location of zero axial mean velocity. In general the mean velocity field is similar for all flows, with differences detected only in a detailed comparison and more pronounced

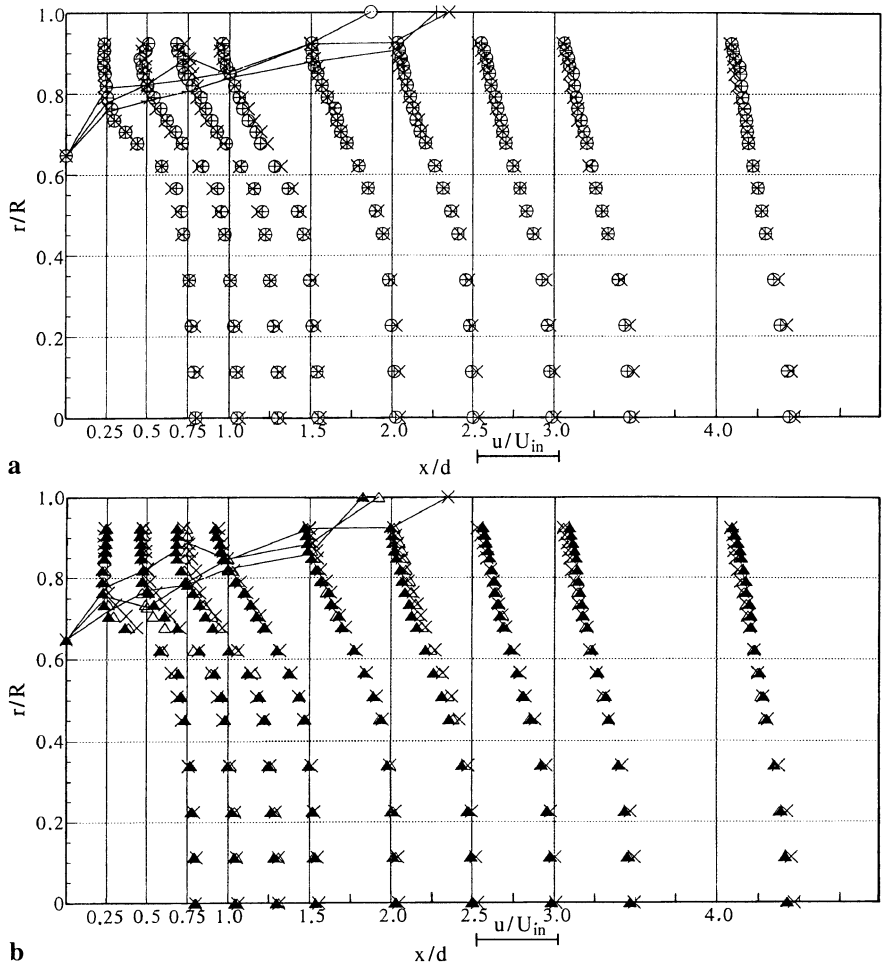

Fig. 6. Normalised mean velocity profiles. **a** × water $Re = 50{,}300$; + water $Re = 135{,}000$; ○ 0.1% xanthan gum $Re_w = 19{,}600$. **b** × water $Re = 50{,}300$; △ 0.2% xanthan gum $Re_w = 19{,}400$; ▲ 0.2% xanthan gum $Re_w = 27{,}200$

when involving higher polymer concentrations. Near the expansion the non-Newtonian solutions have a flatter profile in the core and higher mean velocity gradients in the shear layer. This feature is especially relevant as it contributes to higher turbulence production and thus higher levels of turbulence in the free shear layer, as will be shown in the next section.

At $1.0d$ the differences observed at $0.25d$ remain, i.e. lower velocities in the core for the xanthan gum solutions and slightly more negative velocities in the recirculation, an indication that the region of separated flow could actually be longer. Downstream of reattachment, recovery is lower for the non-Newtonian fluids than for water, as the typical profiles at $4.0d$ indicate.

Upstream of the reattachment flow zone the free shear layer develops in a self-similar way, as do other types of shear layer, except for the first stations where the potential core (originating in the fully-developed pipe flow central region) has not yet been influenced by the growing shear-layer. This can be assessed by the comparison of the axial mean velocity profiles in Fig. 7 with Fig. 8 of Devenport and Sutton (1993). Here we use the coordinate $(r - R_{05})/\delta_\omega$ where R_{05} is the radial location at which $u = 0.5U_0$ and δ_ω is the vorticity thickness. The vorticity thickness δ_ω is defined as

$$\delta_\omega = \frac{U^+ - U^-}{\left(\frac{\partial u}{\partial r}\right)_{\max}} = \frac{U_0}{\left(\frac{\partial u}{\partial r}\right)_{\max}} \tag{5}$$

where U^+ and U^- are the local maximum and minimum velocities in the shear layer, here assumed to be the centreline velocity and zero, respectively. For the other flow conditions not shown a similar behaviour was observed.

The longitudinal variation of the vorticity thickness is also plotted in Fig. 8 and it is clear that on the average it varies as

$$\frac{\delta_\omega}{d} \approx 0.15\frac{x}{d} + 0.1 \tag{6}$$

The gradient of vorticity thickness is thus identical to that reported by Escudier and Smith (1999) but the present values are shifted by 0.1. This shows that the mean and turbulent velocity profiles at the upstream wall increase the initial width of the shear layer, but do not affect its spread rate.

The wall static pressure variation is normalised by $\frac{1}{2}\rho U_{\text{in}}^2$ and profiles are plotted in Fig. 9. Recovery takes longer with water ($9d$ to $10d$) than with the xanthan gum solutions ($\approx 8d$). These

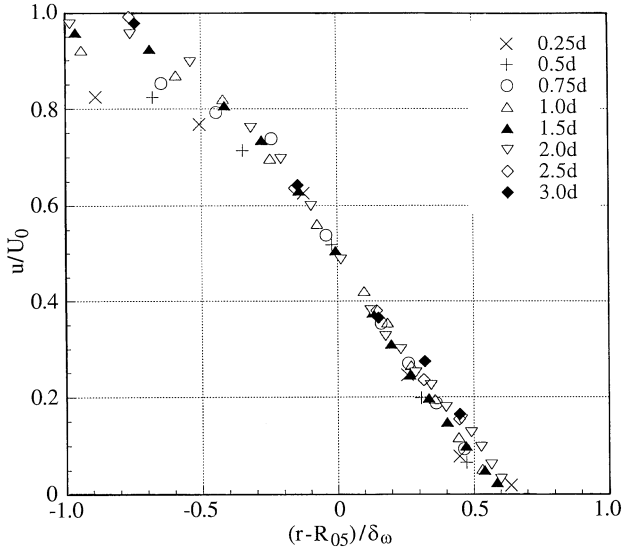

Fig. 7. Profiles of the mean axial velocity in the shear layer for the 0.2% xanthan gum solution at $Re = 19{,}400$

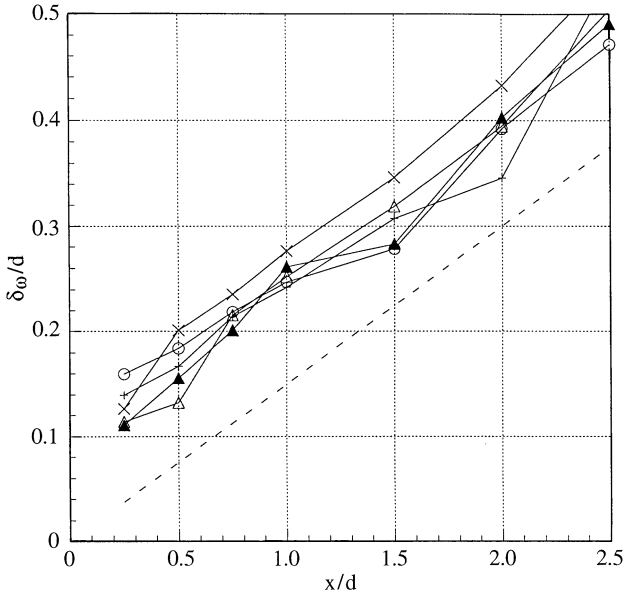

Fig. 8. Longitudinal variation of the vorticity thickness. Symbols as in Fig. 5 and broken line from Escudier and Smith (1999)

are longer distances than observed by Escudier and Smith (1999), who report a recovery distance of about 7*d*. Considering the shorter recirculation lengths measured in this work, the longer pressure recovery lengths are difficult to understand. Pressure variation is very sensitive to the longitudinal mean velocity evolution and small differences in mean and turbulent inlet conditions are bound to have an effect upon C_T. In such a detailed analysis the pressure uncertainty should also be taken into account.

In order to quantify the maximum amount of recovery Fig. 9 includes the theoretical static pressure coefficient C_T given by

$$C_T = 2\beta_1\sigma\left(1-\frac{\beta_2}{\beta_1}\sigma\right) \tag{7}$$

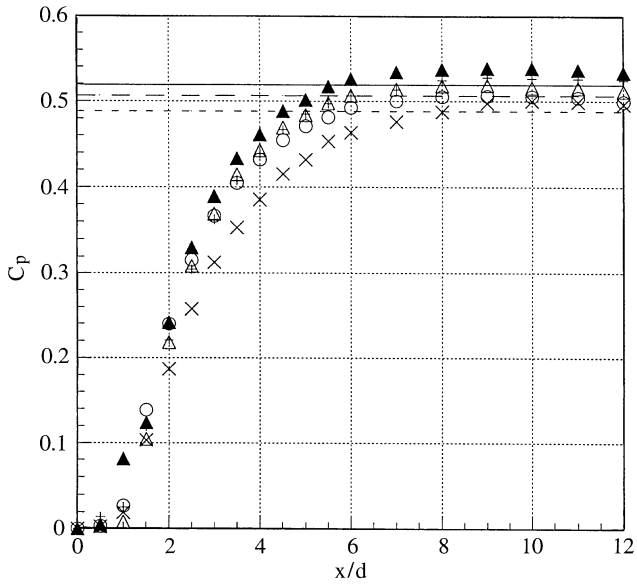

Fig. 9. Longitudinal variation of the total pressure coefficient. Symbols as in Fig. 5. Static pressure coefficient for flat inlet and outlet profiles (short-dashed line) ; static pressure coefficient for present inlet profile $\beta_1 \approx 1.037 \pm 1\%$ and $\beta_2 = 1$ (full line); static pressure coefficient for present inlet profile $\beta_1 \approx 1.037 \pm 1\%$ and $\beta_2 = \beta_1$ (long-dashed line)

where $\sigma = (d/D)^2$ and β_1 and β_2 are fully-developed momentum shape factors upstream and downstream of the expansion ($\beta \equiv \overline{u^2}/\bar{u}^2$, where an overbar denotes area averaging). For each flow, the measured inlet profile allowed quantification of β_1 but measurements were not taken sufficiently downstream to quantify the fully-developed β_2 and two values were thus assumed for this factor: $\beta_2 = 1$ corresponding to a uniform profile, and $\beta_2 = \beta_1$ corresponding to a normalised downstream velocity profile identical to that in the upstream pipe. Note that for polymer solutions exhibiting less drag reduction than the maximum predicted by Virk et al. (1970) the two values of β should differ as this phenomenon depends on both pipe diameter and Reynolds number.

C_T is rather sensitive to β_1 which was determined to be 1.039 and 1.033 for water at $Re_w = 50{,}300$ and 135,000, respectively. For the 0.1XG solution $\beta_1 = 1.036$ and for the 0.2% XG solution at Re_w 19,400 and 27,200 it was 1.044 and 1.037.

The short-dashed line in Fig. 9 represents the theoretical coefficient for uniform inlet and outlet ($C_T = 0.488$), which is exceeded in all cases because of the different inlet profile shape. Taking this into account via β_1 in Eq. (7), the theoretical coefficient is raised by 6% to the full line for $\beta_1 = 1.037$ and $\beta_2 = 1$ ($C_T = 0.519$), and by 3.7% to the long-dashed line for $\beta_1 = \beta_2 = 1.037$ ($C_T = 0.506$). The selected value of β_1 was calculated from the measured inlet velocity profile of 0.2% XG at $Re_w = 27{,}200$ but also corresponds to the average of the various calculated β_1 values. For each combination of β_1 and β_2 the theoretical values of C_T for the other flows are within 1% of the plotted value. The measured C_T's at recovery compare better with the corresponding theoretical value assuming $\beta_1 = \beta_2$ with differences of less than 4% except for the 0.2% XG and water flows at $Re_w = 27{,}200$ and 135,000, respectively. The measured values are higher than the theoretical C_T due to the

pressure gain from the positive friction force at the wall within the recirculation region. It can also be readily concluded that the static pressure coefficients measured at recovery by Escudier and Smith (1999) were lower than the corresponding theoretical values for uniform inlet and outlet velocities.

4.2 Turbulent flow

The maximum values of the normalised normal Reynolds stresses and of the turbulent kinetic energy are listed in Table 3. The decrease in Reynolds number reduces those maxima whereas an increase in polymer concentration only affects the axial component and, by implication, the value of k. For instance, the 0.2% xanthan gum solution flow at $Re_w = 19{,}400$ ($Re = 13{,}400$) has a 10% higher maximum value of the axial Reynolds stress than that of the 0.1% xanthan gum solution at the same Reynolds number but similar values for the two maximum transverse turbulence components.

Comparing with the data of Escudier and Smith (1999) for their 0.2% xanthan gum solution at $Re \approx 26{,}000$, we measured a lower axial and radial maximum turbulence but a higher tangential turbulence which almost compensate each other: the present maximum value of k/U_{in}^2 in 3% higher than theirs (Note that maxima of the three normal Reynolds stresses do not occur at the same location, therefore their sum does not yield the maximum value of k). Inspection of expressions for the production of the Reynolds stresses show that there is no production of $\overline{w'^2}$ and that production of $\overline{u'^2}$ and of $\overline{uv}$ (not measured) are important due to the high mean velocity gradients $\partial u/\partial r$ involved.

$$\text{Production of } \overline{u'^2} = -2\overline{u'^2}\,\partial u/\partial x - 2\overline{u'v'}\,\partial u/\partial r$$

$$\text{Production of } \overline{v'^2} = -2\overline{u'v'}\,\partial v/\partial x - 2\overline{v'^2}\,\partial v/\partial r$$

$$\text{Production of } \overline{u'v'} = -\overline{v'^2}\,\partial u/\partial r - \overline{u'^2}\,\partial v/\partial x \qquad \text{(8a–c)}$$

In Escudier and Smith's (1999) experiments this implies higher $\overline{u'^2}$ values in the shear-layer before the emergence of significant values of turbulence for the other normal components, one of them ($\overline{w'^2}$) can only be obtained by the redistributive mechanism of pressure-strain. In the present measurements there can be an immediate contribution from the other terms of the transport equations of the Reynolds stresses, such as pressure-strain, production of $\overline{v'^2}$ can start as early as production of $\overline{u'^2}$ and there is advection of turbulence from the wall shear-layer in the upstream pipe, thus the turbulent field is less anisotropic and turbulence appears quicker. Therefore, it is not surprising that Escudier and Smith's values of maximum $\overline{v'^2}$ are lower than ours by 20%, but that they have higher $\overline{u'^2}$. Their less intense radial transport of momentum leads to increased recirculation lengths.

The variation of the turbulent maximum quantities with the Reynolds number is also at a contrast: here they decrease with Reynolds number whereas in Escudier and Smith they increase.

The whole turbulent flow field is shown in the contour plots of the normalised axial, tangential and radial normal Reynolds stresses of Figs. 10, 11 and 12, respectively. The x- and r-axis have different scalings and a dashed line, marking the end of recirculation, was added to help in the comparisons. At a first sight the various plots in each figure look identical, but closer inspection shows the following differences:

1) Everywhere in the flow field the axial Reynolds stress is the highest, followed by the tangential and then the radial components, in agreement with the findings of Escudier and Smith (1999) and Castro and Pinho (1995) and matching what was observed before with the corresponding maximum values;
2) The loci of the maximum normal Reynolds stresses of the non-Newtonian solutions are upstream of the corresponding loci for the Newtonian flows, and for some cases those maxima also attain higher values, i.e, the initial development of turbulence in the shear layer is faster for the xanthan gum solutions than for the water flows;
3) On moving downstream the Reynolds stresses for the non-Newtonian solutions decay at a faster rate than those of the Newtonian flows, and this is particularly clear for the radial component and less so for the tangential component. This has also been found by Castro and Pinho (1995) for tylose solutions.

The more intense non-Newtonian turbulence dampening is due to increased turbulence dissipation and is evident at a later stage of the shear layer (in the vicinity of reattachment zone and further downstream), but is not strong enough and happens too late to reverse the effects of earlier higher turbulence and inlet condition in shortening the recirculation bubble. This pronounced effect of the polymer additive upon transverse turbulence has been observed previously in sudden expansion free-shear layers with tylose solutions (Castro and Pinho, 1995) and in jets with polyacrylamide and polyethylene oxide solutions (Berman and Tan, 1985) and is also typical of wall-dominated turbulent flows, as explained above.

The relevance of the inlet condition is emphasized in the comparison between the present measurements of water and xanthan gum flows by analysing again, in more detail the turbulence production mechanisms. The flatter axial mean velocity profiles of the xanthan gum solutions at inlet in Fig. 5 can lead to higher mean velocity gradients in the free shear layer (Fig. 6). The Reynolds shear stress was not measured due to optical limitations, but it is expected that in the upstream pipe it will be lower than for the Newtonian fluids because of the axial-transverse turbulence decoupling associated with drag reduction (Willmarth et al. 1987). So, production of $\overline{u'^2}$ via the second term on the right-hand side of Eq (8a) could be similar but probably is lower than that of Newtonian fluids. Since turbulent dissipation with non-Newtonian fluids is more intense than that of Newtonian fluids, presumably because of elongational properties (Oliveira and Pinho, 1998), high values of $\overline{u'^2}$ (and similar values of $\overline{v'^2}$ and $\overline{w'^2}$) can only be understood on the basis of another strong source of $\overline{u'^2}$ such as advection from upstream, which feeds turbulence into the shear layer but also enhanced production of $\overline{u'^2}$ via the first term on rhs of Eq. (8a). Thus, the anticipated higher levels of turbulence with non-Newtonian fluids in the initial part of the shear layer, especially in the radial direction, result to a large extent from the upstream turbulent flow field and enhance radial momentum transfer which reduces the recirculation length.

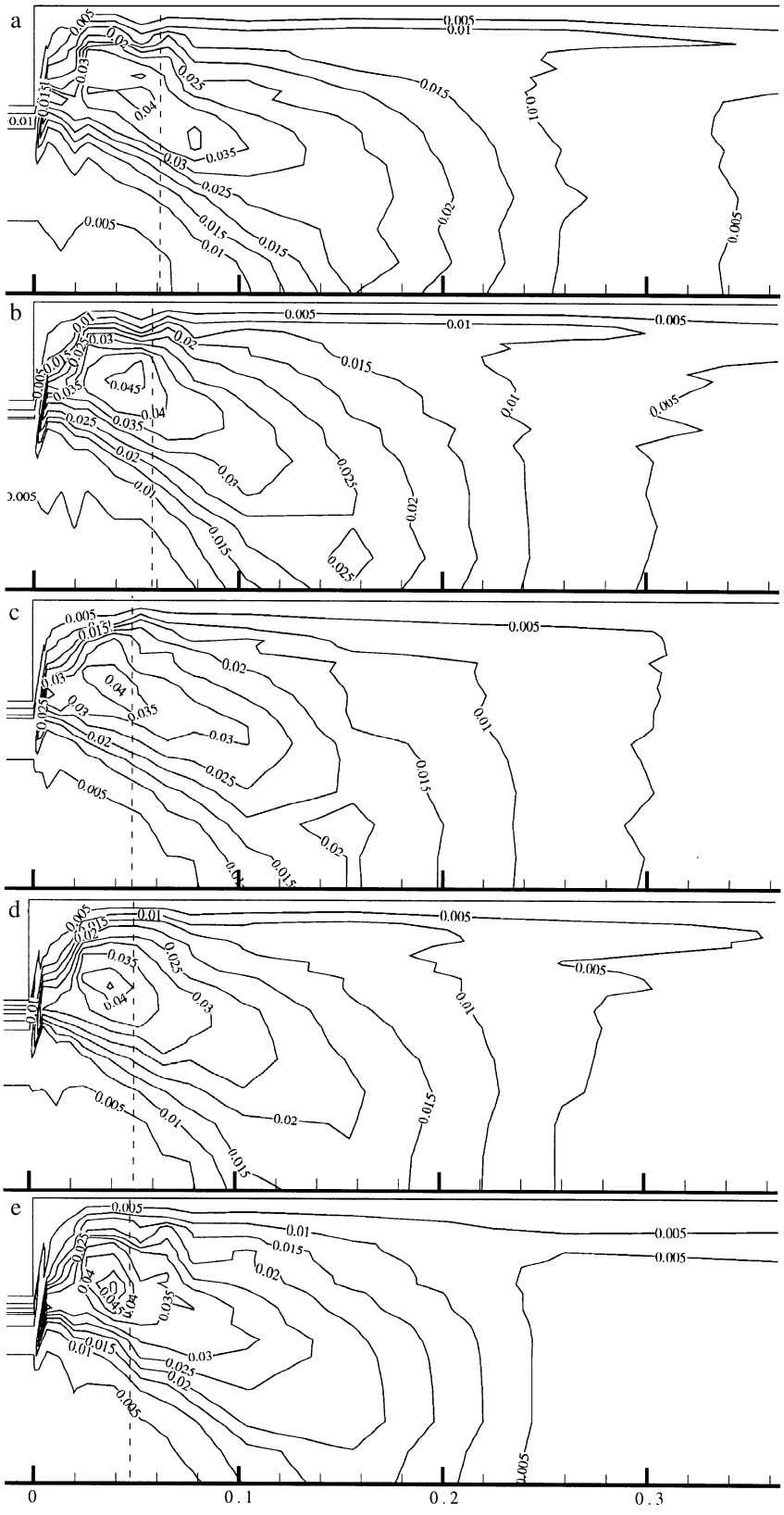

Fig. 10. Contour plots of the normalised axial normal Reynolds stress: **a** water $Re_w = 50{,}300$; **b** water $Re_w = 135{,}000$; **c** 0.1% XG $Re_w = 19{,}600$; **d** 0.2% XG $Re_w = 19{,}400$; **e** 0.2% XG $Re_w = 27{,}200$

5 Conclusions

Measurements of the mean and turbulent flow fields downstream of a sudden expansion were carried out for a Newtonian and two elastic xanthan gum aqueous solutions at upstream wall Reynolds numbers (Re_w) between 19,000 and 135,000, and for fully-developed inlet flow. These measurements were compared with those of Escudier and Smith (1999), who used similar fluids but a flat velocity entry flow of low turbulence.

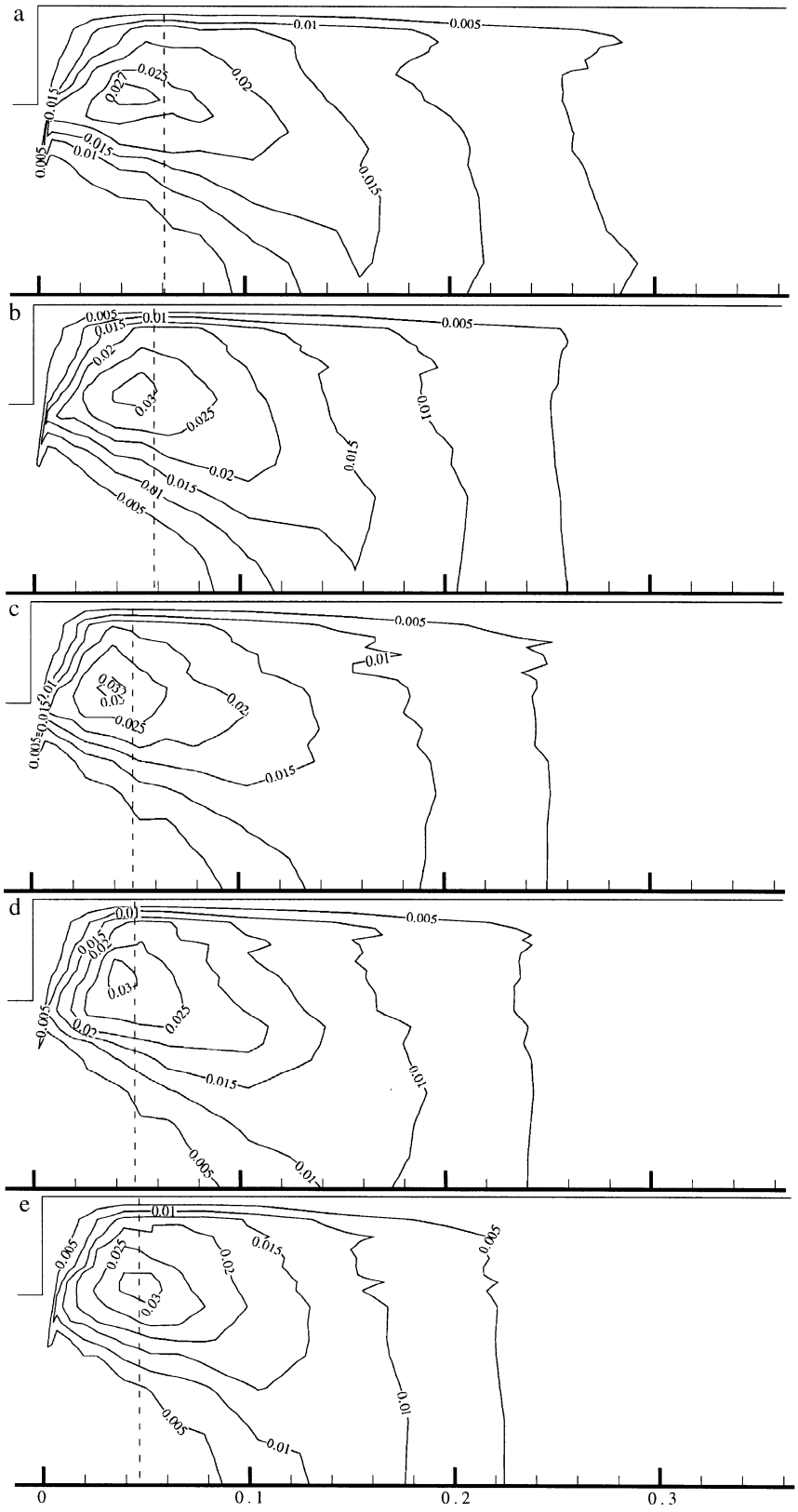

Fig. 11. Contour plots of the normalised tangential normal Reynolds stress: **a** water $Re_w = 50{,}300$; **b** water $Re_w = 135{,}000$; **c** 0.1% XG $Re_w = 19{,}600$; **d** 0.2% XG $Re_w = 19{,}400$; **e** 0.2% XG $Re_w = 27{,}200$

The shear layer downstream of the sudden expansion for both Newtonian and non-Newtonian fluids exhibited self-similar characteristics to those of a truly free-shear layer and the vorticity thickness varied as $\delta_\omega/d = 0.15x/d + 0.1$.

In our measurements, addition of polymer resulted in drag reduction in the upstream pipe flow which was characterised by a flatter axial mean velocity and higher axial normal Reynolds stresses in the wall region. The higher turbulence at

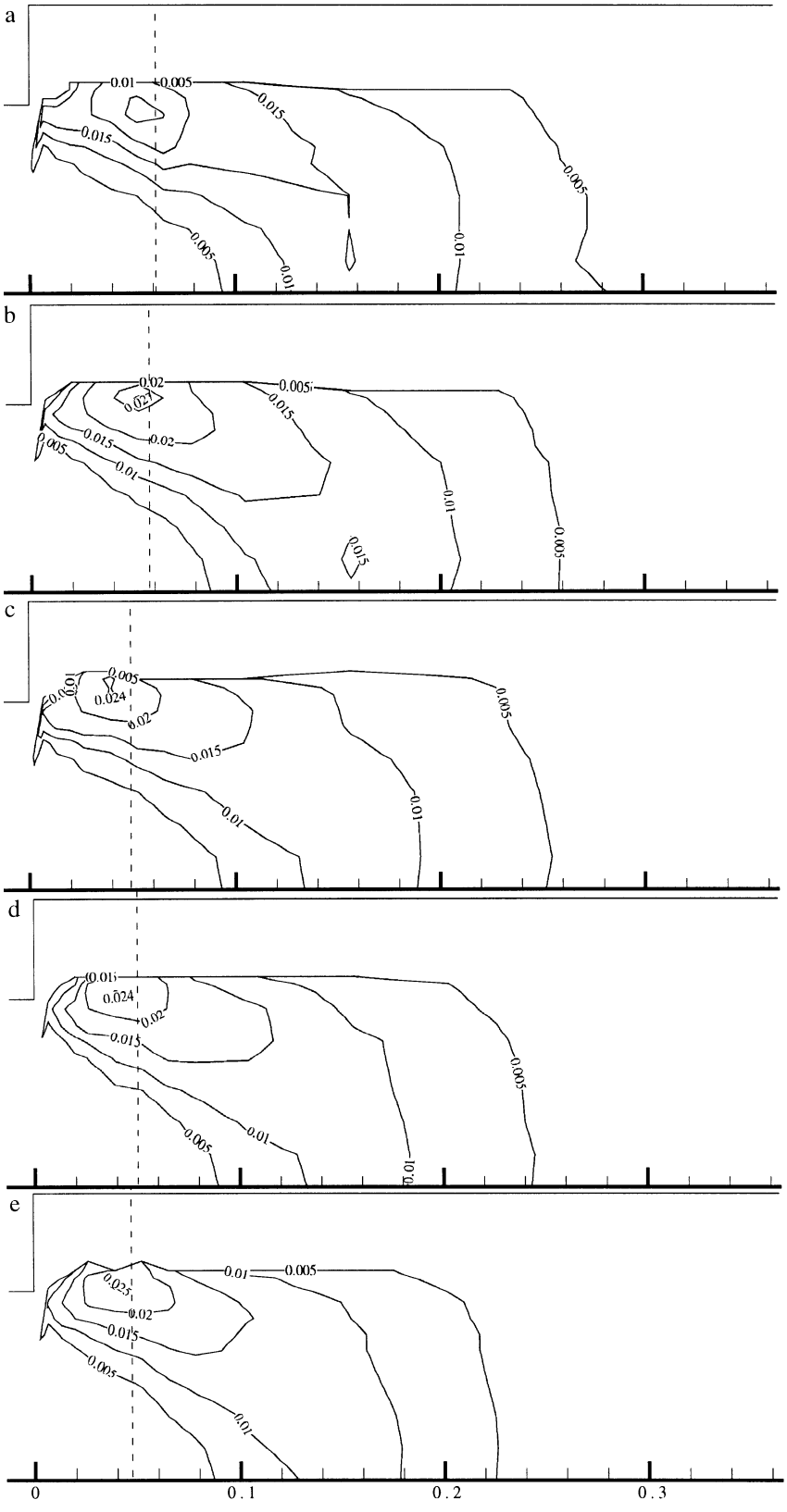

Fig. 12. Contour plots of the normalised radial normal Reynolds stress: **a** water $Re_w = 50{,}300$; **b** water $Re_w = 135{,}000$; **c** 0.1% XG $Re_w = 19{,}600$; **d** 0.2% XG $Re_w = 19{,}400$; **e** 0.2% XG $Re_w = 27{,}200$

the inlet pipe wall region was advected downstream by the mean flow and resulted in higher axial turbulence in the shear layer downstream of the expansion plane, but especially in maximum values of the Reynolds stresses occurring earlier than for the Newtonian flows. The main consequence was the shortening of the recirculation bubble by an average amount of 20% relative to the water flows.

For a low turbulence flat velocity inlet, on the other hand, Escudier and Smith report a stronger turbulence anisotropy than we do, with 20% lower maximum values of $\overline{v'^2}$ and 16%

higher maximum values of $\overline{u'^2}$ for the 0.2% xanthan gum solution at an identical Reynolds number, which is the result of the absence of a high turbulence wall layer in the upstream pipe. The absence of the upstream boundary layer is a lower vorticity thickness and radial turbulence in the shear-layer and a longer recirculation zone.

References

Berman NS; Tan H (1985) Two-component laser-doppler velocimeter studies of submerged jets of dilute polymer solutions. AIChEJ 2: 208–215

Castro OS; Pinho FT (1995) Turbulent expansion flow of low molecular weight shear-thinning solutions. Exp Fluids 20: 42–55

Devenport WJ; Sutton EP (1993) An experimental study of two flows through an axisymmetric sudden expansion. Exp Fluids 14: 423–432

Drikakis D (1997) Bifurcation phenomena in incompressible sudden expansion flows. Phys Fluids 9: 76–87

Escudier MP; Smith S (1999) Turbulent flow of Newtonian and shear-thinning liquids through a sudden axisymmetric expansion. Exp Fluids, in press

Escudier MP; Gouldson IW; Jones DM (1995) Flow of shear-thinning fluids in a concentric annulus. Exp Fluids 18: 225–238

Escudier MP; Gouldson IW; Pereira AS; Pinho FT (1998) On the consistency of the rheology of dilute shear-thinning elastic fluids. Submitted to J. Non-Newt. Fluid Mech

Gyr A; Bewersdorff H.-W. (1995) Drag reduction of turbulent flow by additives, Fluid mechanics and its application series, Dordrecht, Kluwer Academic Publishers

Khezzar L; Whitelaw JH; Yianneskis M (1985) An experimental study of round sudden expansion flows. Proc 5th Symp. on Turb. Shear Flows, Cornell University: 5–25

Laufer (1954) The structure of turbulence in fully developed pipe flow. NACA Report 1174: 1–18

Lawn CJ (1971) The determination of the rate of dissipation in turbulent pipe flow. J Fluid Mech 37: 477–505

Oliveira PJ; Pinho FT (1997) Pressure drop coefficient of laminar Newtonian flow in axisymmetric sudden expansions. Int J Heat and Fluid Flow 18: 518–529

Oliveira PJ; Pinho FT (1998) A qualitative assessment of the role of a third invariant of the rate of deformation tensor dependent viscosity on turbulent flow. J Non-Newt Fluid Mech 78: 1–25

Pak B; Cho YI; Choi SU (1990) Separation and reattachment of non-Newtonian fluid flows in a sudden expansion pipe. J Non-Newt Fluid Mech 37: 175–199

Pak B; Cho YI; Choi SU (1991) Turbulent hydrodynamic behavior of a drag-reducing viscoelastic fluid in a sudden expansion pipe. J Non-Newt Fluid Mechanics 39: 353–373

Pereira AS; Pinho FT (1994) Turbulent pipe flow characteristics of low molecular weight polymer solutions. J Non-Newt Fluid Mech 55: 321–344

Pinho FT (1990) Velocity characteristics of polymer solutions in ducts. PhD thesis, University of London, UK

Pinho FT; Whitelaw JH (1990) Flow of non-Newtonian fluids in a pipe. J Non-Newt Fluid Mech 34: 129–144

Rouse H; Ince S (1957) History of hydraulics, Dover Publications Inc. 1963 edition, New York

Stieglmeier M; Tropea C (1992) A miniaturized, mobile laser-doppler anemometer, Applied Optics, 111: 4096–4099

Tokaty GA (1971) A history and philosophy of fluid mechanics, New York, Dover Publications Inc. 1994 edition

Willmarth WW; Wei T; Lee CO (1987) Laser anemometer measurements of Reynolds stress in a turbulent channel flow with drag reducing polymer additives. Physics of Fluids, 30: 933–935

Virk PS; Mickley HS; Smith KA (1970) The ultimate asymptote and mean flow structure in Tom's phenomena. ASME J Appl Mech 92: 488–493